On Extended Finite Element Method (XFEM) for Modelling of Organ Deformations Associated with Surgical Cuts

Lara M. Vigneron[1], Jacques G. Verly[1], and Simon K. Warfield[2]

[1] Signal Processing Group
Department of Electrical Engineering and Computer Science
University of Liège, Belgium
[2] Surgical Planning Laboratory
Brigham and Women's Hospital and Harvard Medical School
Boston, USA

Abstract. The Extended Finite Element Method (XFEM) is a technique used in fracture mechanics to predict how objects deform as cracks form and propagate through them. Here, we propose the use of XFEM to model the deformations resulting from cutting through organ tissues. We show that XFEM has the potential for being the technique of choice for modelling tissue retraction and resection during surgery. Candidates applications are surgical simulators and image-guided surgery. A key feature of XFEM is that material discontinuities through FEM meshes can be handled without mesh adaptation or remeshing, as would be required in regular FEM. As a preliminary illustration, we show the result of XFEM calculation for a simple 2D shape in which a linear cut was made.

1 Introduction

Neurosurgeons plan surgery from patients' structural and functional images. During surgery, neuronavigation systems display the positions of surgical instruments in preoperative images. However, the brain deforms in the course of a surgery. These deformations occurs principally following the opening of the dura, the drainage of the cerebrospinal fluid (CSF), the retraction of tissues and the successive resections of, say, a tumor [5]. The usefulness of neuronavigation systems is then limited: the current brain shape no longer corresponds to that of the preoperative images. Intraoperative image acquisition can partially circumvent this limitation by capturing the new configuration of the brain, but such image acquisition is limited in signal-to-noise ratio and spatial resolution by the time constraints of the surgical procedure. Additionally, not all imaging modalities (particularly functional ones) are available intraoperatively. Consequently, intraoperative monitoring and surgical navigation can be significantly improved by estimating the deformation of the brain and projecting preoperative imaging data into alignment with the subject brain.

S. Cotin and D. Metaxas (Eds.): ISMS 2004, LNCS 3078, pp. 134–143, 2004.

Nonrigid registration techniques are numerous. One approach is to use biomechanical models to encapsulate the mechanical properties and behavior of the brain. We use intraoperative MRI images in order to compute the displacements of the cortical and ventricular surfaces of the brain. The displacement field then drives the brain model in place of the forces. Deformations throughout the brain are calculated using the finite element method (FEM) with a linear elastic behavior law [18]. Our approach and implementation are similar to those of Ferrant [5][7][6].

Virtually all past studies on brain deformation modelling have focused on the brain shift at an early stage of the procedure, before significant resection has taken place. The precision achieved in the prediction of displacements in this particular context are good, with for instance, landmark matching errors of 0.8 ± 0.4 mm at the surface of the brain and 1.1 ± 0.7 mm for the interior (mean±standard deviation) [7], which is comparable to the size of the voxels.

In comparison, modelling of retraction and resection is still in its infancy. There have been limited investigations of the forces involved in these two surgical tasks [10]. There has also been an effort to create a so-called "smart retractor" capable of measuring forces intraoperatively; this device has already shown promising results [1]. Intraoperative images will be very useful when used in conjunction with this device. Ferrant et al. [6] has used intraoperative MRI and captured brain deformation in the presence of resection, but the model of resection simply consisted of clipping the deformed brain with the resection cavity.

Conventional FEM has serious limitations for modelling the tissue discontinuities associated with the resection of a tumor. The displacement field that is the solution of the finite-element (FE) calculation must be continuous inside each FE. Furthermore, the displacement at any node may take on only one value. Consequently, the modelling of a discontinuity requires that discontinuity boundaries be aligned with boundaries of the elements and that nodes lying on these boundaries be duplicated.

Extensive work has been performed in the domain of surgical simulation on the problem of cutting of a FE mesh [13][3]. Most of the proposed solutions and algorithms are based on a subdivision method [2][9][12][8][13]. All elements intersected by the cut are divided into sub-elements in order to create a boundary of finite elements aligned with the cut. The subdivision is subject to the constraint of a good aspect ratio for the new elements.

The main drawback of this method is the rapid growth of the numbers of nodes and elements in the mesh. In addition to the subdivision calculation, the larger mesh size increases the computation time, and it is challenging to maintain computationally efficient parallel data structures as the mesh evolves. Of course, it is important to keep in mind that real-time performance is absolutely essential for surgical navigation and simulation.

Alternative methods have been evaluated to avoid these dramatic changes in the mesh. For example, the mesh may be adapted to the geometry of the cut: some nodes are selected, and they are then relocated to cling as best as possible

to the cut geometry. However, an offset can remain between the boundary formed by these relocated nodes and the cut. Element degeneracies can also happen [14]. Depending on the method used, the distortion of the mesh can produce elements with unacceptably large aspect ratios. One solution is a remeshing, but this will in turn lead to an increase in the computation time [15].

We propose a new method for cutting meshes in arbitrary ways without mesh adaptation or remeshing, thereby avoiding all of the above drawbacks. This method allows the object to be modeled by finite elements without explicitly meshing the cut surfaces. Discontinuities can then be arbitrary located with respect to the underlying FE mesh. In addition, no remeshing is required when the discontinuity changes shape. Other appealing features of the method are that the FE framework and its advantages (sparsity and symmetry) are retained and that a single-field (displacement) variational principle is used. This method is called "extended finite element method (XFEM)" and was introduced in 1999 in the field of fracture mechanics for the study of crack and related failures, such as for bridges and airplanes [11].

The paper is organized as follows. In Section 2, we review the basic principles of FEM. In Section 3, we discuss the theory of XFEM. In Section 4, we provide a proof-of-concept simulation for a simple 2D object. Finally, in Section 5, we discuss the role and benefits of XFEM for handling the deformation of the brain in surgery, especially in the presence of significant retraction and resection.

2 Review of Basic FEM Principles

The problem of finding the displacement field $\boldsymbol{u}(\boldsymbol{x})$ such that the weak form of the equations of linear elasticity is satisfied is equivalent to determining the displacement field which minimizes the total deformation energy E

$$E = \frac{1}{2}\int_{\Omega} \boldsymbol{\sigma}\,\boldsymbol{\varepsilon}\,d\Omega - \int_{\Omega} \boldsymbol{b}\,\boldsymbol{u}\,d\Omega - \int_{\Gamma_t} \overline{\boldsymbol{t}}\,\boldsymbol{u}\,d\Gamma. \tag{1}$$

The quantities in (1) are as follows. $\boldsymbol{\varepsilon}(\boldsymbol{x})$ and $\boldsymbol{\sigma}(\boldsymbol{x})$ are the strain tensor and the stress tensor, respectively. $\boldsymbol{b}(\boldsymbol{x})$ is the body force applied to the solid, while $\overline{\boldsymbol{t}}(\boldsymbol{x})$ is the traction force applied to its surface. Ω represent the volume of the solid and Γ_t represents the surface of the solid on which traction is applied.

To solve the linear elastic problem, we need to discretize the equations. In particular, we need an approximation $\boldsymbol{u}^h$ for the displacement field $\boldsymbol{u}$. The FEM approximation is defined by

$$\boldsymbol{u}^h(\boldsymbol{x}) = \sum_{i=1}^{N} \varphi_i(\boldsymbol{x})\boldsymbol{u}_i, \tag{2}$$

where the $\boldsymbol{u}_i$'s are the discrete unknowns to be determined and the φ_i's are basis functions, called shape functions. These functions must obey 2 conditions. First, φ_i has a compact support $\boldsymbol{\omega}_i$, which corresponds to the union of element subdomains connected to node i. Second, we have

$$\varphi_i(\boldsymbol{x}_j) = \begin{cases} 1 & if \quad i = j \\ 0 & if \quad i \neq j \end{cases} \quad on \quad \boldsymbol{\omega}_i, \tag{3}$$

where the $\boldsymbol{x}_i$'s, $i = 1, ..., N$, are the coordinates of the nodes.

Equations (2) and (3) yield the following property

$$\boldsymbol{u}^h(\boldsymbol{x}_i) = \sum_{i=1}^{N} \varphi_i(\boldsymbol{x}_i)\boldsymbol{u}_i = \boldsymbol{u}_i. \tag{4}$$

The FEM unknown $\boldsymbol{u}_i$ can be shown to be the displacement field value at the node $\boldsymbol{x}_i$. The FEM displacement field interpolates nodal displacements.

Finally, the introduction of the FE approximation (2) in the minimization of (1) leads to the following system of linear equations

$$\boldsymbol{K}\boldsymbol{u} = \boldsymbol{f} \quad or \quad \boldsymbol{K}_{ij}\boldsymbol{u}_i = \boldsymbol{f}_i \quad i, j = 1, ..., n, \tag{5}$$

where

$$\boldsymbol{K}_{ij} = \int_{\Omega} \boldsymbol{B}_i^T \boldsymbol{H} \boldsymbol{B}_j \, d\Omega \quad with \quad \mathbf{B}_i = \begin{pmatrix} \frac{\partial \varphi_i}{\partial x} & 0 & 0 \\ 0 & \frac{\partial \varphi_i}{\partial y} & 0 \\ 0 & 0 & \frac{\partial \varphi_i}{\partial z} \\ \frac{\partial \varphi_i}{\partial y} & \frac{\partial \varphi_i}{\partial x} & 0 \\ 0 & \frac{\partial \varphi_i}{\partial z} & \frac{\partial \varphi_i}{\partial y} \\ \frac{\partial \varphi_i}{\partial z} & 0 & \frac{\partial \varphi_i}{\partial x} \end{pmatrix}, \tag{6}$$

$$\boldsymbol{f}_i = \int_{\Omega} \mathbf{b}\varphi_i \, d\Omega + \int_{\Gamma_t} \overline{\mathbf{t}}\varphi_i \, d\Gamma \tag{7}$$

and H is Hooke's tensor. The final step is to solve (5) for the displacement $\boldsymbol{u}_i$. One can then use (2) to align preoperative and intraoperative images.

3 Introduction to Basic XFEM Principles

3.1 Fundamental Equations

This section introduces the fundamental ideas of XFEM. For details regarding the theory and various implementation issues, the reader should consult, e.g., [11][17][4][16].

The key of this method is to create a new displacement-field approximation by enriching the FE approximation (2), that is by multiplying some of the FE nodal shape functions by discontinuous functions. This enrichment can be made to take local form by only enriching those nodes whose support intersect a region of interest. We have

$$\boldsymbol{u}^h(\boldsymbol{x}) = \sum_{i \epsilon I} \varphi_i(\boldsymbol{x})\boldsymbol{u}_i + \sum_{i \epsilon J} \varphi_i(\boldsymbol{x}) \sum_{j=1}^{n^{E_i}} g_j(\boldsymbol{x})\boldsymbol{a}_{ji}. \tag{8}$$

The quantities in (8) are as follow. The φ_i's are the FE shape functions and the g_j's are the XFEM enrichment functions. We denote by I the set of all N nodes in the domain, and by J the subset of I corresponding to the n^E enriched nodes. $\boldsymbol{u}_i$ and $\boldsymbol{a}_{ji}$ are nodal DOFs and n^{Ei} denotes the number of enrichment functions for node i. The additional DOFs $\boldsymbol{a}_{ji}$ are associated with nodes that are enriched.

An important consequence of the XFEM function enrichment is that the approximation does not interpolate nodal displacements for enriched nodes $\boldsymbol{x}_i$, i.e.,

$$\boldsymbol{u}^h(\boldsymbol{x}_i) = \sum_{i \epsilon I} \varphi_i(\boldsymbol{x}_i)\boldsymbol{u}_i + \sum_{i \epsilon J} \varphi_i(\boldsymbol{x}_i) \sum_{j=1}^{n^{E_i}} g_j(\boldsymbol{x}_i)\boldsymbol{a}_{ji} = \boldsymbol{u}_i + \sum_{j=1}^{n^{E_i}} g_j(\boldsymbol{x}_i)\boldsymbol{a}_{ji} \neq \boldsymbol{u}_i. \quad (9)$$

3.2 Choice of Enrichment Functions and Enriched Nodes

We denote by Γ_d the crack surface. Any function that is discontinuous across Γ_d can be used to model an arbitrary discontinuity in $\boldsymbol{u}^h(\boldsymbol{x})$. The simplest choice is a piecewise-constant function that changes sign at the boundary Γ_d, the Heaviside function

$$H(\boldsymbol{x}) = \begin{cases} 1 & for \quad (\boldsymbol{x} - \boldsymbol{x}^*).\boldsymbol{e}_n > 0 \\ -1 & for \quad (\boldsymbol{x} - \boldsymbol{x}^*).\boldsymbol{e}_n < 0 \end{cases} \quad (10)$$

where $\boldsymbol{x}$ is a sample point of the solid, $\boldsymbol{x}^*$ is the point on the crack that is the closest to $\boldsymbol{x}$, and $\boldsymbol{e}_n$ is the outward normal to the crack at $\boldsymbol{x}^*$ [1] (Fig. 1(a)). The nodes that are enriched by this function are those for which the support intersects the crack.

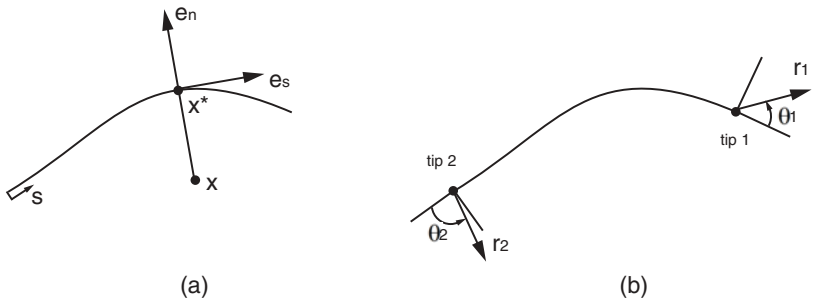

Fig. 1. (a) Coordinates of the Heaviside function corresponding to the crack discontinuity (2D case). (b) Local coordinates of the crack-tip enrichment functions (2D case).

However, this function is not sufficient to model accurately the tip of the crack when this tip terminates inside an element. Indeed, the node and so all of its support is enriched. Consequently, the crack would be modeled as though the "crack-tip" was extended till it intersects the element edge.

[1] "Outward" is defined in an obvious way based upon the relative positions of $\boldsymbol{x}$ and Γ_d.

Consequently, nodes whose supports containing a crack-tip are not enriched with the Heaviside function, but with specific crack-tip enrichment functions that ensure that the crack terminates precisely at the location of the crack-tip. The crack-tip enrichment relies on functions that incorporate the radial and angular behavior of the asymptotic crack-tip displacement field, which is two-dimensional by nature (Fig. 1(b))

$$\{F_l(r,\theta)\}_{l=1}^{4} = \{\sqrt{r}sin(\frac{\theta}{2}), \sqrt{r}cos(\frac{\theta}{2}), \sqrt{r}sin(\frac{\theta}{2})sin(\theta), \sqrt{r}cos(\frac{\theta}{2})sin(\theta)\}, \quad (11)$$

where r and θ are the local polar-coordinates[2].

The XFEM approximation for a single pair of crack and crack-tip is thus

$$\boldsymbol{u}^h(\boldsymbol{x}) = \sum_{i=1}^{N} \varphi_i(\boldsymbol{x})\boldsymbol{u}_i + \sum_{j\epsilon J} \varphi_j(\boldsymbol{x})H(\boldsymbol{x})\boldsymbol{a}_j + \sum_{k\epsilon K} \varphi_k(\boldsymbol{x})(\sum_{l=1}^{4} F_l(\boldsymbol{x})\boldsymbol{c}_k^l). \quad (12)$$

The quantities in (12) are as follows. The $\boldsymbol{u}_i$'s are the nodal DOFs associated with the continuous part of the FE solution, the $\boldsymbol{a}_j$'s are the nodal enriched DOFs associated with the Heaviside function, and the $\boldsymbol{c}_k^l$'s are the nodal enriched DOFs associated with the crack-tip functions. I is the set of all nodes in the mesh. J is the set of nodes whose shape function support is cut by the crack interior. K is the set of nodes whose shape function support is cut by the crack-tip ($\boldsymbol{x}_c$). With D denoting the crack geometry, we thus have the formal definitions

$$K = \{k \epsilon I \ : \ \boldsymbol{x}_c \epsilon \varpi_k\} \qquad J = \{j \epsilon I \ : \omega_j \ \cap \ D \neq \emptyset, j \notin K\}, \quad (13)$$

where ω_k denotes the compact support of the node k and ϖ_k its closure. The above equations can easily be generalized to several pairs of cracks and crack-tips.

To obtain the discrete XFEM equations equivalent to the FEM equations (5)-(7), we must substitute the approximation expression (12) in the total-energy expression (1) and minimize the resulting expression.

Additional details regarding the equations can be found in [17].

While FEM requires a remeshing and the duplication of nodes along the crack to take into account any discontinuity, the XFEM requires identification of nodes belonging to the sets J and K and the computation of the stiffness matrice with enrichment fonctions. Because of added nodal DOFs in XFEM, stiffness matrix is larger than in FEM.

4 Proof-of-Concept 2D XFEM Simulation

To evaluate the abilities and potential of XFEM for surgical guidance and simulation, we have performed preliminary tests on simple 2D objects such as rectangles and ellipses containing a line-segment crack discontinuity. An exploratory

[2] The first function is discontinuous on the crack faces.

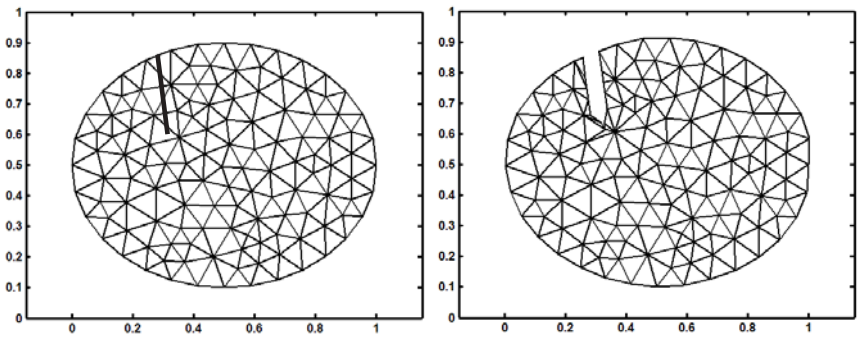

Fig. 2. (a) Mesh and crack geometries before deformation. (b) Results of XFEM when displacements (14) and (15) given in text are applied along the crack.

program was written in Matlab. The Matlab PDE toolbox was used, but only to initialize a triangular mesh from a domain boundary.

The inputs to the program are the mesh definition and the crack geometry (Fig. 2(a)). One begins by identifying the mesh elements that are fully intersected by the crack and the mesh elements that contain a crack-tip. The number of DOFs for each node is then defined: 2 for a non-enriched node, 4 for a Heaviside-function-enriched node or 10 for a near-tip-functions-enriched node. As with FEM, each elementary stiffness matrix is computed, taking into account the enrichment functions, and the global stiffness matrix is subsequently assembled. The application of force or displacement constraints is performed in similar ways in both FEM and XFEM.

To illustrate the method, we have chosen to constrain the displacement along the (linear) crack. We have applied a displacement of $(0.0266, 0.0103)$ and $(-0.0266, -0.0103)$[3] to each intersection, with the mesh, of the right and left crack lips, respectively. The intersection of the crack with the element containing the crack tip was left free (i.e., no displacement was imposed) to avoid having excessive constraints near the tip. Indeed, we have noticed that element flipping can sometimes happen in this situation.

The application of this displacement constraint is straightforward in XFEM. For the intersection ($\boldsymbol{x}_{int}$) of an element defined by 3 nodes enriched with the Heaviside fonction, the relation between the nodal DOFs[4] are

$$\begin{cases} \varphi_1(\boldsymbol{x}_{int})\, u_{x1} + \varphi_1(\boldsymbol{x}_{int})\, a_{x1} + \varphi_2(\boldsymbol{x}_{int})\, u_{x2} + \varphi_2(\boldsymbol{x}_{int})\, a_{x2} = 0.0266 \\ \varphi_1(\boldsymbol{x}_{int})\, u_{y1} + \varphi_1(\boldsymbol{x}_{int})\, a_{y1} + \varphi_2(\boldsymbol{x}_{int})\, u_{y2} + \varphi_2(\boldsymbol{x}_{int})\, a_{y2} = 0.0103, \end{cases} \tag{14}$$

[3] Each point is of the form (x, y), with the x and y axes being respectively horizontal and vertical in Fig. 2.

[4] We consider the intersection lying on the element boundary between node 1 with DOFs $(u_{x1}, u_{y1}, a_{x1}, a_{y1})$ and node 2 with DOFs $(u_{x2}, u_{y2}, a_{x2}, a_{y2})$.

for the right lip where the Heaviside function (10) is equal to 1. Similarly, we have

$$\begin{cases} \varphi_1(\boldsymbol{x}_{int})\, u_{x1} - \varphi_1(\boldsymbol{x}_{int})\, a_{x1} + \varphi_2(\boldsymbol{x}_{int})\, u_{x2} - \varphi_2(\boldsymbol{x}_{int})\, a_{x2} = -0.0266 \\ \varphi_1(\boldsymbol{x}_{int})\, u_{y1} - \varphi_1(\boldsymbol{x}_{int})\, a_{y1} + \varphi_2(\boldsymbol{x}_{int})\, u_{y2} - \varphi_2(\boldsymbol{x}_{int})\, a_{y2} = -0.0103, \end{cases} \tag{15}$$

for the left lip where the Heaviside function (10) is equal to -1. The result of these displacement constraints is an opening of the crack, which is illustrated in Fig. 2(b).

This example confirms that XFEM can elegantly and efficiently take into account (crack) discontinuities in the study of the mechanical properties of objects. In particular, remember that no mesh adaptation or remeshing is required. In contrast with FEM, solution displacement fields can now contain discontinuities inside the finite elements. Observe that the triangles that appear to have been added in Fig. 2(b) were added for display purposes only. They are needed to show the new boundary of the crack. However, none of these additional nodes or elements are involved in the XFEM calculation.

5 Conclusions and Perspectives

XFEM is particularly well adapted to deal with the general problem of cutting through a 2D or 3D finite-element mesh. This is required to deal with discontinuities, i.e., cracks or cuts. The main feature of XFEM is that it can deal with discontinuities without having to perform computationally-expensive mesh adaptation or remeshing. Note that the technique applies to multiple discontinuities that have arbitrary locations and shapes.

The implication for surgical guidance and simulation are clear and significant. In surgery, XFEM could be very useful in the modelling of retraction and resection, each of these surgical procedures inducing discontinuities in tissues. The pieces of information we need are the discontinuity geometry and the displacement contraints along the organ surfaces and the discontinuity boundary. The incision surface allowing the insertion of the retractor can be determined by tracking. It can also be inferred from an intraoperative MRI image showing the retraction pathway. The displacements caused by the retractor can be calculated from distances between segmented brain boundaries along the retraction path and the calculated incision surface. The modelling of resection is more complicated given that the brain can swell during this surgical procedure and that this swelling is not visible in intraoperative images. However, the difficult task of removing finite elements according to the boundary of resected areas can be done accurately with XFEM. Indeed, all elements falling entirely in the resected area can be removed. With the remaining elements, we can precisely specify the boundary of the resected cavity by adding discontinuous functions to nodes located along this boundary, which allows us to cancel the presence of the elements on the resected side of the boundary.

The next step in our XFEM work will be the application and evaluation of the ideas and techniques proposed above to MRI images of a phantom submitted to retraction and resection.

References

1. Asha Balakrishnam, Daniel F. Kacher, Alexander Slocum, Corey Kemper, and Simon K. Warfield. Smart retractor for use in image guided neurosurgery. *2003 Summer Bioengineering Conference, June 25-29, Sonesta Beach Resort in Key Biscayne, Florida.*
2. D. Bielser and M. H. Gross. Interactive simulation of surgical cuts. In Pacific Graphics 2000 IEEE Computer Society Press, editor, *Proceedings of Pacific Graphics 2000*, pages 116–125, Hong Kong, China, October 2–5 2000.
3. S. Cotin, H. Delingette, and N. Ayache. A hybrid elastic model allowing real-time cutting, deformations and force-feedback for surgery training and simulation. *The Visual Computer*, 16(8):437–452, 2000.
4. John E. Dolbow. *An Extended Finite Element Method with Discontinuous Enrichment for Applied Mechanics.* PhD Dissertation, Northwestern University, 1999.
5. Matthieu Ferrant. *Physics-based Deformable Modeling of Volumes and Surfaces for Medical Image Registration, Segmentation and Visualization.* PhD thesis, Université catholique of Louvain, Telecommunications Laboratory, Louvain-la-Neuve, Belgium, April 2001.
6. Matthieu Ferrant, Arya Nabavi, Benoit Macq, Ferenc A. Jolesz, Ron Kikinis, and Simon K. Warfield. Registration of 3D intraoperative MR images of the brain using a finite element biomechanical model. *IEEE Trans. Medical Imaging*, 20(12):1384–1397, Dec. 2001.
7. Matthieu Ferrant, Arya Nabavi, Benoit Macq, Ron Kikinis, and Simon Warfield. Serial registration of intra-operative MR images of the brain. *Medical Image Analysis*, 6:337–359, December 2002.
8. Clément Forest, Hervé Delingette, and Nicholas Ayache. Cutting simulation of manifold volumetric meshes. In Takeyoshi Dohi and Ron Kikinis, editors, *Medical Image Computing and Computer-Assisted Intervention (MICCAI'02)*, volume 2488 of *LNCS*, pages 235–244, Tokyo, September 2002. Springer Verlag.
9. F. Ganovelli, P. Cignoni, C. Montani, and R. Scopigno. A multiresolution model for soft objects supporting interactive cuts and lacerations. *Computer Graphics Forum*, 19(3):271–282, 2000.
10. B. K. Lamprich and M. I. Miga. Analysis of model-updated MR images to correct for brain deformation due to tissue retraction. *Medical Imaging 2003: Visualization, Image-guided Procedures and Display: Proc. of the SPIE*, 5029:552–560, 2003.
11. N. Moës, J. Dolbow, and T. Belytschko. A finite element method for crack growth without remeshing. *International Journal for Numerical Methods in Engineering*, 46:131–150, 1999.
12. A. Mor and T. Kanade. Modifying soft tissue models: Progressive cutting with minimal new element creation. In Scott L. Delp, Anthony M. DiGioia, and Branislav Jaramaz, editors, *Medical Image Computing and Computer-Assisted Intervention (MICCAI'00)*, pages 598–607, Pittsburgh, Pennsylvania, October 2000. Springer Verlag.
13. Han-Wen Nienhuys. *Cutting in deformable objects.* PhD thesis, Institute for Information and Computing Sciences, Utrecht University, 2003.
14. Han-Wen Nienhuys and A. Frank van der Stappen. A surgery simulation supporting cuts and finite element deformation. In Wiro J. Niessen and Max A. Viergever, editors, *Medical Image Computing and Computer-Assisted Intervention (MICCAI'01)*, pages 153–160, Utrecht, The Netherlands, October 2001. Springer Verlag.

15. D. Serby, M. Harders, and G. Székely. A new approach to cutting into finite element models. In Wiro J. Niessen and Max A. Viergever, editors, *Medical Image Computing and Computer-Assisted Intervention (MICCAI'01)*, pages 425–433, Utrecht, The Netherlands, October 2001. Springer Verlag.
16. N. Sukumar, N. Moës, T. Belytschko, and B. Moran. Extended Finite Element Method for three-dimensional crack modelling. *International Journal for Numerical Methods in Engineering*, 48(11):1549–1570, 2000.
17. N. Sukumar and J.-H. Prévost. Modeling Quasi-Static Crack Growth with the Extended Finite Element Method. Part I: Computer Implementation. *International Journal of Solids and Structures*, 40(26):7513–7537, 2003.
18. Jacques G. Verly, Lara Vigneron, Nicolas Petitjean, Christophe Martin, Raluca Guran, and Pierre Robe. 3D nonrigid registration and multimodality fusion for image-guided neurosurgery. *Fusion 2003, Proceedings of the 6th International Conference on Information Fusion, Cairns, Australia*, 2003.